Modified-SST for Uniaxial Characterization of Electrical Steel Sheets Under Controlled Induced Voltage and Constant Stress

Benjamin Joseph Mailhé, Laurent Didier Bernard, Laurent Daniel, *Member, IEEE*, Nelson Sadowski, *Senior Member, IEEE*, and Nelson Jhoe Batistela, *Senior Member, IEEE*

***Abstract*— This article details the development of a uniaxial magnetomechanical bench that allows measuring the effect of constant tensile and compressive stress on the magnetic properties of electrical steel sheets. Following international standards for magnetic measurements, this work proposes reasonable modifications of a single-sheet-tester set up to provide a reliable magnetomechanical characterization of the material. The magnetic circuit and the excitation and control techniques employed are described. Specifications concerning magnetic measurements are also offered, alongside mechanical considerations regarding the antibuckling fixture developed to allow the application of compressive stress. Finally, results obtained for various stress levels and frequencies are validated and analyzed. Among other results, the proposed bench allows observing the negative impact of compressive stress on magnetic properties of nonoriented steel, as well as the positive effect of mild tensile stress.**

***Index Terms*— Magnetic field measurement, magnetomechanical behavior, single-sheet tester (SST), standard testing.**

I. Introduction

OVER the past few decades, intensive research has been realized to improve magnetic losses management and mitigation in transformers and rotating machines. In particular, investigations lead the path to a better physical understanding of hysteretic losses in electrical steel sheets. From these works, a phenomenon overlooked for a long time resurfaced: the magnetomechanical coupling that can be broadly defined as the interdependence of the mechanical and magnetic states of a ferromagnetic material. Two particular occurrences of this coupling are the magnetostriction—the spontaneous deformation of a magnetic material exposed to a magnetizing field—and its reciprocal effect, which consists in the alteration of the magnetic properties, such as permeability and losses, when imposing mechanical stress onto a material [1]–[4].

This article offers a detailed presentation of a magnetomechanical bench that allows measuring with precision the effect of tensile and compressive stress on steel sheets' magnetic properties.

After a brief overview of the different sources of mechanical loads that can emerge during the lifetime of electrotechnical machinery, the modified-single-sheet-tester (SST) proposition will be introduced and compared to similar works present in the literature.

A. Sources of Mechanical Loads

Most electrical steel sheets used in electrotechnical machinery are Fe–Si-based. Their properties can be affected throughout their whole lifetime as a consequence of the magnetomechanical coupling, whether during the conformation stages (residual stress) or their use in the machines (applied/external stress). As examples of processes generating mechanical deformations during the fabrication of steel sheets, it is possible to enunciate the lamination process itself [5], stamping and other cutting methods [6], and bad or incomplete thermal treatments [7]. Mounting laminated sheets together to form the cores of rotating machines and transformers can also generate significant forces, as presented in [8] and [9]. Finally, it is important to keep in mind that every kind of apparatus will induce a generation of the stress of magnetic as well as nonmagnetic origins. If the first ones can be neglected most of the time due to their low intensity, the second ones can reach high levels [8]. For example, in motors and generators, inertial forces coupled to sharp geometries can generate local stresses of high intensity [10], [11].

B. Magnetomechanical Bench Proposal

Various proposals of experimental benches can be found in the literature. Some of them offer slight modifications of SST testers in order to deliver rapid knowledge of standard magnetic material properties to design engineers, as in [12]. Occasionally, magnetomechanical benches allowing the application of various magnetic and mechanical conditions can also

Manuscript received November 13, 2019; revised May 2, 2020; accepted June 18, 2020. Date of publication July 2, 2020; date of current version November 10, 2020. This work was supported in part by the Coordenação de Aperfeiçoamento de Pessoal de Nível Superior (CAPES) Foundation and in part by the Conselho Nacional de Desenvolvimento Científico e Tecnológico (CNPq) and CAPES/Comité Français d'Evaluation de la Coopération Universitaire et Scientifique avec le Brésil (COFECUB) Foundations under Project 88881.191763/2018-01. The Associate Editor coordinating the review process was Kamel Haddadi. *(Corresponding author: Benjamin Joseph Mailhé.)*

Benjamin Joseph Mailhé, Laurent Didier Bernard, Nelson Sadowski, and Nelson Jhoe Batistela are with the Grupo de Conceição e Análise de Dispositivos Electromagnéticos (GRUCAD)/Department of Electrical and Electronic Engineering (EEL)/Technological Center (CTC), Universidade Federal de Santa Catarina, Florianópolis 88040-900, Brazil (e-mail: ben.mailhe@gmail.com).

Laurent Daniel is with the Laboratoire de Génie Électrique et Électronique de Paris, CentraleSupélec, Centre National de la Recherche Scientifique (CNRS), Université Paris-Saclay, 91192 Gif-sur-Yvette, France, and also with the Laboratoire de Génie Électrique et Électronique de Paris, Centre National de la Recherche Scientifique (CNRS), Sorbonne Université, 75252 Paris, France.

Color versions of one or more of the figures in this article are available online at http://ieeexplore.ieee.org.

Digital Object Identifier 10.1109/TIM.2020.3006682

be found. However, SST standards are generally not followed. In [13], for example, the setup exposed does not allow compressive stress using standard sheet thickness, which is, thus, increased. This configuration, also found in [14], can induce the undesired Eddy current effects in the sheet thickness, despite allowing the application of high compressive loads. Furthermore, the rig used does not respect SST standards, notably regarding the sample size and, thus, the material representativity [15]. A solution to buckling was proposed by Rekik *et al.* [16], using a specific coating technique, which eventually allows imposing bidirectional stress onto a sample excited by an alternating field. In this case, the main drawback lies in the magnetic excitation method that is realized through imposed current on the primary coil—this method that does not allow the analysis of losses through usual segregation method based on sinusoidal induction waveform. Bench using a rotational magnetic field and uniaxial stress can also be found [17], as well as fully bidirectional benches [18] and even more complex multidirectional setups [19]. In all those studies, concerns exist regarding notably the magnetic excitation application and its control. Finally, it is important to stress that a modified-SST proposal by Kanada [20] allows applying uniaxial tensile and compressive stress onto a thin sheet subjected to collinear alternated magnetic excitation, in a quite similar way the present proposal does. However, few details are furnished regarding the control of this excitation, and no information is given regarding the antibuckling system used to avoid bending of thin sheets tested under compression.

Following this idea, this article offers the description of a dedicated tool able to quantify with precision the impact of uniaxial mechanical stress on the magnetic properties of steel sheets. It is designed in order to comply with international standards for magnetic measurements set as a key point [21]–[23], thus avoiding the shortcoming found in other bench proposals. To achieve excitation and control requirements, a power inverter and a closed-loop nonlinear analog control based on the sliding modes theory were used to feed the magnetic excitation of an SST (see Section II). This system allows the generation of an excitation signal so that the induced voltage obtained on the secondary coil of the magnetic circuit corresponds to a user-defined reference (see Section II-B). Dedicated sensors and conditioning-amplifying techniques were developed to measure the low-intensity responses of both the rig and tested material (see Section III). Specific mechanical features were also designed to avoid the buckling of thin sheets under compressive stress (see Section IV) and, thus, realize the measurements in magnetically and mechanically controlled conditions (see Section V).

This way, in Section II, the design of the SST magnetic core will be presented alongside the excitation and control systems required for standardized magnetic testing.

II. Single-Sheet Tester

Among the diverse techniques commonly employed to measure magnetic properties of laminated sheets (e.g., the Epstein frame and toroidal core), it was decided to base the experimental test bench on the SST method. This approach allows a relatively easy implementation of mechanical loads while being widely accepted in the scientific and industrial community as a reliable apparatus. Indeed, SST offers easier implementation and a lower material cost than other methods while furnishing high precision results, versatility, and representativity. The design simplicity of such an experimental bench could be seen as a drawback since it limits the magnetic excitation to one unidirectional configuration, but it, nevertheless, matches perfectly with the fixed goal of studying simple configurations of magnetomechanical coupling in a standardized fashion while allowing easy replication.

TABLE I
International Standards Requirements & Recommendations for SST Systems [21]–[23]

Parameters	Requirements/Recommendations
Configuration	Recommended: 2 C-shaped yokes
Internal length Li_y	Minimum 220 mm [21], [23] Optimal 450 mm [22]
Width l_y	Minimum 30 mm [21]
Height h_y	90 to 150 mm [22] Construction limitations [21], [23]
Pole faces thickness e_y	25 mm for regular material 19 mm for high perm. mat. [21]
Air-gap g	Max. 5 μm [22]
Yokes manufacturing	GO Fe-Si/Ni-Fe alloy Stacked or bent core
Losses $W_{y,tot}$	Max. 1 W/kg at 1,5 T and 50 Hz
Primary winding	At least 80% of internal length Rec. 400 turns on 1 or more layers
Secondary winding	Around the tested specimen
Supply system	Control of v_{ind} (sin.) required
Steel sheets dimensions	$l_{sh} = l_y$ (avoids field waviness) $L_{sh} \geq Li_y + 2e_y \gg l_{sh}$
Mounting	Upper-yoke support needed

A. Magnetic Circuit

The first conception step consisted in defining the general magnetic characteristics of the modified SST. One aspect of it is the geometry of the magnetic core (or yoke) that is used to magnetize the sheet and, thus, of the sheet geometry itself. Another one is the magnetic response of the core. Various points were taken into account in order to define these parameters, the most important ones being the adequacy with international standards for SST development and the precision that could be obtained on the measurement. Considerations regarding the geometry and properties of the magnetic circuit can be found in various international standards, with slight differences from one to another [21]–[23]. Table I summarizes those requirements, while Fig. 1 helps understanding their geometrical aspects.

Taking them into account, along with the adaptations necessary to mechanical stress application, the magnetic circuit was designed and realized, as described in the following. A configuration with two horizontal C-yokes was chosen (see Figs. 1 and 2); despite inducing more complex instrumentation due to geometrical restrictions, this configuration mostly compensates the effect of induced current pools generated by

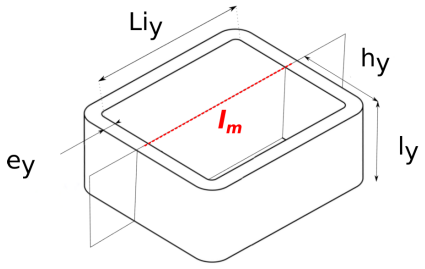

Fig. 1. Schematic of the double-yoke magnetic circuit and magnetic path l_m (red dotted line).

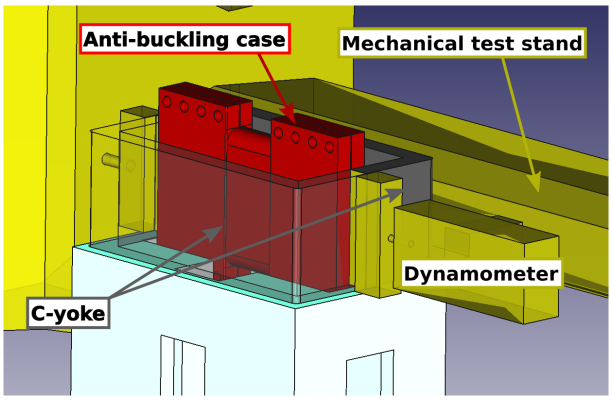

Fig. 2. Partial scheme of the modified SST configuration for the magneto-mechanical coupling analysis.

the magnetic flux circulating from the yoke poles into the tested sample at a right angle, apart from homogenizing the magnetic field within the system [24]. Horizontal disposition of the yokes was chosen since it avoids overstressing the tested sheet because of an upper yoke weight and so dispense the use of a suspension system while lowering undesired magnetomechanical effects on contact faces. Finally, as the tested sheet is sustained perpendicularly to the floor, the risk of self-buckling is lowered, while only simple support is needed for the antibuckling, as shown in Fig. 2.

The yokes were made of one single strip of grain-oriented (GO) Fe–Si material, rolled onto itself along its rolling direction to form a rectangular bent core. The resulting transformer was then sliced in half, and the cuts carefully polished in order to have a better surface quality, lowering roughness and then potential air gap, as well as preventing any short circuits between the superposed strip parts. Those aspects, coupled with the oxidation insulation of the original strip and the final epoxy coating of the yoke, enable obtaining a magnetic circuit with high performance (low total losses at interest frequencies) and, thus, a low impact on the measurement.

The yokes material showing a high permeability when excited in its RD; it was possible to reduce the pole face width e_y from 25 to 19 mm (see Table I). Other dimensions were then taken in agreement with the less restrictive standards (ASTM 804 [21]) having in mind the accommodation with the mechanical excitation system and the desired experiments to be made on the SST. In that sense, Li_y was fixed to 220 mm for the magnetic system to fit within the stroke

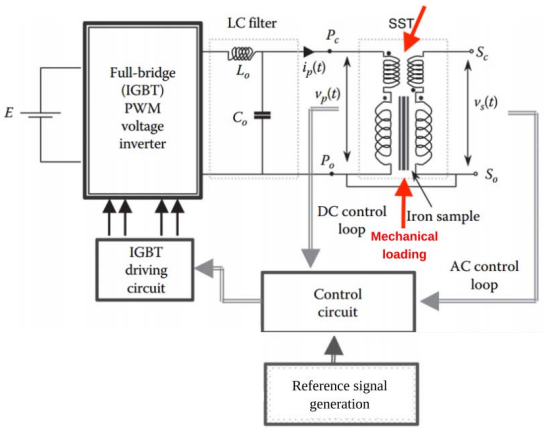

Fig. 3. Functional diagram of the magnetic excitation and control of the developed test bench.

of the universal tension/compression test stand used for this study. Width l_y was chosen equal to 100 mm so that a local field sensor can be accommodated in the middle of the steel sheet, far from the specimen sides and then from potential residual stress generated during the cutting process. The average steel sheets dimensions used in this article are $320 \times 100 \times 0.5$ mm^3, the extra length allowing the fixation of the strip for mechanical loading. It should be stressed that the system could be used for thin sheets with other thicknesses, as detailed in Section IV.

B. Control and Excitation

As noted in Table I, international standards recommend to control the system in order to ensure a sinusoidal induced voltage v_{ind} on the secondary coil (B-coil). Indeed, when approaching saturation, material behavior shows high nonlinearity. Imposing a sinusoidal waveform on the induced voltage, thus, allows proper characterization and permits the direct application of loss segregation models [25]. In this study, the voltage waveform induced on the secondary coil is, thus, maintained sinusoidal (relative error on the form factor $e_r < 1.2\%$), while the magnetizing current is adjusted in function of nonlinearities present within the material and the SST in general.

The aforementioned control is realized using an experimental test bench developed in [26]. In this system, the excitation of the primary coil is realized through a single-phase voltage inverter fed by a bilevel pulsewidth modulation (PWM) connected to full-bridge insulated-gate bipolar transistors (IGBTs). The exciting module is coupled to a nonlinear closed-loop control (feedback control) based on the sliding modes theory; the whole system consisting, thus, of an analog sliding mode control (SMC). A functional diagram of the test rig, including the control and excitation components, can be found in Fig. 3. This system allows the user to ensure the form and amplitude of the induced voltage by the mean of a user-defined reference v_{ref}. This signal is generated through a dedicated Virtual Instrument (VI) developed on the LabView platform. The bridge between the software and the hardware is made by a PCI-61160E board

from National Instruments. The error between v_{ind} and v_{ref} is analogically calculated and the magnetizing current i_P applied accordingly, minimizing the integrated error between the two signals.

The primary coil configuration chosen for the test bench slightly deviates from the one recommended by international standards. The modification was decided due to the necessity of easily changing the steel sheet within the antibuckling case (see Section IV) and to simplify the access to local field sensors (see Section III-B). In that sense, the primary coil consists of two identical coils wound around the yokes and linked in series. Each coil possesses 350 turns of AWG 20 coated copper wire (for a total of $N_P = 700$ turns), regularly spaced along the 220 mm of the yokes internal length on two layers. With such configuration, it can be expected that a slightly stronger leakage flux will be visible on the magnetic field measurement apparatus, matter discussed in Section III-B.

In Section III, methods and tools employed in this work to obtain reliable induction and magnetic field measurements are detailed.

III. Measurement of Magnetic Quantities

It is necessary to measure two main quantities in order to properly describe the behavior of a magnetically excited material: the magnetic field H [A/m] at the sheet surface and the mean induction in the sample cross section B [T]. Both quantities are linked by expressions (1)–(4). It is important to note that since the developed test bench only allows unidirectional magnetic excitation, all related material quantities are expressed in terms of scalars

$$B = \mu_0(H + M) \tag{1}$$

$$= \mu H \tag{2}$$

$$= \mu_r \mu_0 H \tag{3}$$

$$W_{\text{tot}} = \frac{1}{m_v} \int_{B|_{t=0}}^{B|_{t=T}} H\,dB \tag{4}$$

where $\mu_0 = 4\pi\ 10^{-7}$ H/m is the void permeability, M is the magnetization of the tested specimen [A/m], μ is the material permeability [H/m], μ_r is the material relative permeability, m_v is the material volumetric density [kg/m^3], T is the period associated with $B(t)$ [s], and W_{tot} [J/kg] is the total energy lost over one period per unit mass.

A. Magnetic Induction

Material induction is calculated from the induced voltage v_{ind} measured by an inductive sensor, commonly known as secondary coil or B-coil, as shown in (5). Cumulative discrete integration is realized using the common trapezoidal rule with a small time-step (defined by the chosen sampling frequency). This coil is wound around the sample center of an effective magnetic section S and consists of 375 turns of AWG 27 copper wire equally spread on a single layer. The small dimension of the B-coil in comparison with the yoke internal length lowers the impact of leakage flux near the pole faces on the measure. As mentioned in Section II-B, the signal measured on the B-coil is maintained sinusoidal using the SMC

$$B(t) = -\frac{1}{N_S S} \int_0^t v_{\text{ind}}(t')dt'. \tag{5}$$

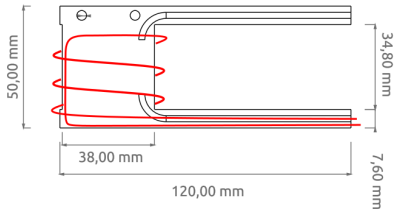

Fig. 4. H-coil support geometry used in this work—support thickness: 0.60 mm; final thickness: ≈1.6 mm.

B. Local Magnetic Field

Following measurement recommendations based on Poynting's theorem and developed in [27], the magnetic field is here considered at the air/sheet interface. Direct local measurement of the magnetic field is, thus, realized due to flat air-cored coils, commonly known as H-coils, as shown in Fig. 4. Such a measurement method leads to a better approximation of the actual magnetic field present at the laminated sheet surface while overcoming most of the limitations of the indirect method based on the current flowing through the exciting coil. It also avoids the need for SST calibration since direct magnetic field sensors are not subjected to errors that arise because of the yoke and air gaps [28].

1) Principle: The direct measurement is based on the conservation of the tangential component of the magnetic field [24]. Because of this phenomenon, the sensor shows a response to the varying external magnetic field $H(t)$ given by (6), where $v_H(t)$ is the induced voltage in the terminals of the sensor, S_H is the mean section of the coil, and N_H is the number of turns. The field can then be calculated from the coil signal because of expression (7)

$$v_H(t) = N_H \mu_0 S_H \frac{dH(t)}{dt} \tag{6}$$

$$H(t) = \frac{1}{N_H \mu_0 S_H} \int_0^t v_H(t')dt'. \tag{7}$$

2) H-Coil Parameters: Due to its conception, the winding is limited in size and, thus, shows parasite capacitances along its length. These, as well as the self-inductance of the coil and its resistance, can be modeled with lumped parameters. Analyzing the equivalent circuit, it can be shown that the sensor operates as a second-order low-pass filter, with a cut-off frequency depending on its construction parameters. The H-coil characteristics were then chosen taking into account this information, the limitations of available tools, and the dimensions of the magnetic circuit. Table II shows the constructive parameters of the sensor. The H-coil thickness was chosen as low as possible—0.6 mm without the winding and a total of ≈1.6 mm with the winding and its protective layer–due to the restriction of the antibuckling system (see Section IV). All H-coils and amplifiers were calibrated due to a Helmholtz coil [29].

TABLE II
MEAN CHARACTERISTICS OF H-COIL SENSORS

Wire	AWG 45 PU-coated copper
N_H	2000 turns
Number of layers	3
S_H	$\approx 3,2.10^{-5}$ mm^2
Resistance R	$\approx 1650\ \Omega$
Impedance L	$\approx 3,3.10^{-3}$ H
Parasitic capacitance	$\approx 1,2.10^{-9}$ F
Sensor cut-off frequency	≈ 80 kHz
External capacitor	10 nF
Global cut-off frequency	≈ 26 kHz

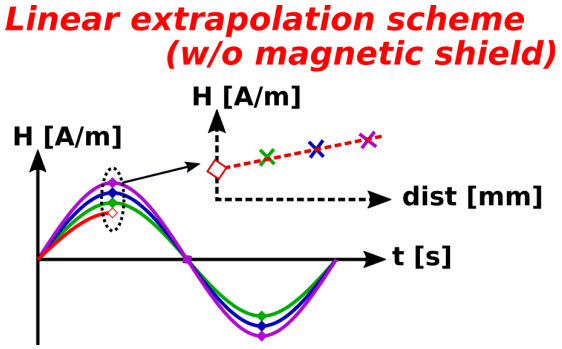

Fig. 5. Scheme of the employed linear regression and extrapolation principle based on the measure of three H-coil sensors placed at different sheet surface distances, without magnetic shield.

3) H-Coils Spatial Configuration: Even if the use of an H-coil enhances the representativeness of magnetic field measurements in SST, it does not guarantee its precision. Indeed, the distance between the tested sheet surface and the sensor influences obtained results [24]. Studies have notably demonstrated that in the present configuration—two C-yokes with symmetric primary coils—and in presence of a magnetic shield, the field intensity measured by an H-coil decreases linearly with the increasing distance. When using the same configuration but without shielding, the intensity slightly increases due to the leakage flux measured, following once more a linear pattern [24], [30].

Thus, three H-coils placed at different distances from the sheet surface are used to measure the magnetizing field in this work. A numerical regression is realized using those various measurement points in order to obtain a better precision on the magnetic field intensity at the sample surface, as schematically shown in Fig. 5. The distances between sensors were defined taking into account the mechanical resistance requirements of the antibuckling fixture needed for compressive tests.

Furthermore, a configuration without a shield is chosen. Such choice was motivated by the fact that low-frequency tests are realized, so it is important to maximize the field amplitude perceived by the sensors in order to increase the signal-to-noise ratio obtained on all H-coils [30].

4) Signal Conditioning: The induced voltage on the H-coil terminals is composed of the information signal and interferences. To acquire the information signal with the best signal-to-noise ratio, an analog filter was employed prior to the amplification stage. This consists of the use of a low-pass filter with an adequate bandwidth in order to attenuate the high-frequency components since they can be responsible for the saturation of amplifiers. The filter used in this article was a second-order low-pass filter made with the sensors coil and an external capacitor. This way, it is possible to change the cutoff frequency by switching the external capacitor value (see Table II).

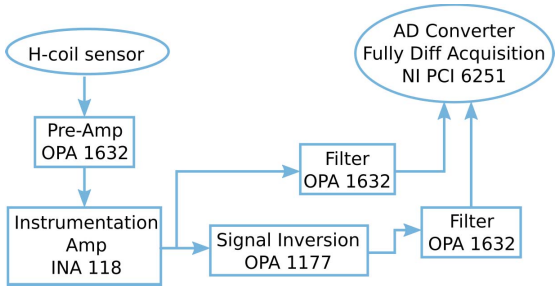

Fig. 6. H-coil fully differential amplifier scheme.

Besides the high noise in the induced voltage on the sensor terminals, the signal also presents a low amplitude in the order of tens of millivolts. Because of this, it is fundamental to implement an amplification stage in the analog conditioning system. Taking advantage of the differential nature of the output signal of the sensor, an instrumentation amplifier was used. Its topology allows high gain and high common-mode noise rejection. In this article, an INA118P from Texas Instruments was used in addition to a fully differential operational amplifier OPA1632 acting as a preamplifier. After the amplification stage realized by the INA118P, the output signal is inverted using an OP1177, thus obtaining a fully differential amplified signal. Each "side" of it then passes through active filters using an OPA1632 in order to recover a cleaner output signal, with high gain and low phase. A scheme of the amplification process can be found in Fig. 6.

C. Data Acquisition and Treatment

The digitalization of the data originated from the magnetic field and induction sensors is realized through a PCI6251 board coupled with a BNC2111 socket by National Instruments. In order to simultaneously acquire the voltage from the secondary coil and the three amplified signals from H-coil sensors, a dedicated VI was developed in LabView.

Posttreatment of obtained experimental results is partially realized in another external LabView program, which is able to treat multiple files at once. The linear extrapolation of magnetic fields calculated from H-coil signals is also automatically done point by point, and the extrapolated surface tangential field, thus, recovered. The user can choose whether or not to apply an additional numerical filter and treat the data in a global or per period fashion in order to reduce the noise in the magnetic field measurement [31]. Finally, B–H loops are exported for a second treatment in the dedicated routines developed under GNU Octave [32].

In Section IV, the design of the antibuckling fixture and the mechanical system allowing the application of tensile and compressive stress onto the sheet sample is presented.

IV. Mechanical Loading

In order to realize the mechanical excitation of the steel sheet while magnetically exciting it, a mechanical stress system was added to the test bench. The lamination, presenting a really thin thickness in comparison with the other dimensions, is subject to buckling under compressive stress. An antibuckling fixture was, thus, developed to avoid the occurrence of such phenomena.

A. Antibuckling Case Development

For this part, the sheet thickness was fixed to 0.35 mm for the diverse calculations: from one side, it represents the lowest sample thickness commonly obtainable, and from the other side, it is the configuration that will buckle the fastest and then will induce a higher level of stress for a given mechanical compression because of the sheet high out-of-plane deformation rate. To define the antibuckling system geometry, mechanical analytical and numerical calculations were employed. An advanced structural analysis was notably realized using the finite element software *code_aster* [33], as briefly described in the following.

First, it was fundamental to define the critical load from which the sheet starts to buckle as well as its oscillation modes. From this point, the so-called postcritical buckling numerical analysis was realized to observe the influence of the sheet material (purely elastic or bilinear elastoplastic) on the mechanical behavior of the laminated strip. Once verified that the material stays in elastic regime while buckling, rigid contact was included in the simulation and the pressure induced by the deforming sheet on the surface collected. Extrapolation techniques then allowed the determination of the maximum pressure to which the antibuckling system would be subjected to a compressive stress of 20 MPa.

The geometry of the antibuckling case was then defined accordingly (see Section IV-B) taking into account the necessity of allowing the entrance of sheets having various thicknesses and the requirements regarding the magnetic measurement tools. Further calculations were realized to ensure the mechanical stability of the system. A conservative value of the calculated contact pressure was chosen ($\sigma_{\text{contact}} = 0.1$ MPa) and applied uniformly on the case surface. This allowed defining the material in which it should be realized, remembering that it must be magnetically and electrically neutral.

B. Antibuckling Case Realization

The antibuckling case can be seen in Fig. 7: it consists of a two-part case of polyether ether ketone (PEEK) material, conferring to the system excellent geometrical stability, high shear modulus, and low friction. Moreover, the material is nonmagnetic and electrically insulating.

The geometry allows the insertion of the sheet having different thicknesses due to an adjustable clearance, resulting in a "sandwiched" laminated sample. Once the sheet is in its position, a set of sixteen (16) nylon screws are used to fix the system setup. A calculation (Kellerman–Klein formula) was realized in order to define the torque necessary to be applied on each screw in order to compensate for the contact pressure of the buckling plate without overstressing the sheet in its thickness. Indeed, this stress could alter the material response to the magnetomechanical excitation, which is to be avoided.

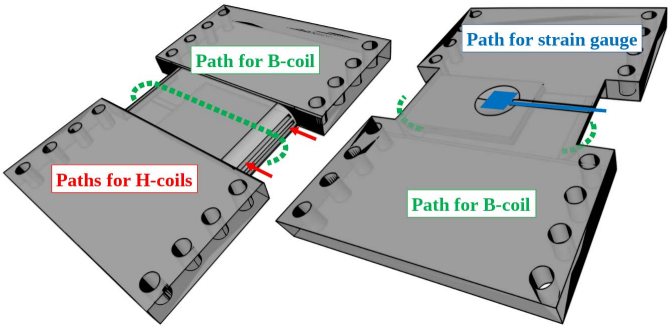

Fig. 7. Final antibuckling case design.

Some features were added in order to conveniently place up to four H-coils—or other thin local probes, such as ARM or the Hall effect sensors—at various distances from the sheet surface. In Fig. 7, two of them are visible as cuts on the case side (red arrows). Around the middle of the case, the secondary coil is wound, enveloping the H-coils. A space dedicated to the positioning of the strain gauge was also foreseen.

C. Unidirectional Tension and Compression System

In order to apply mechanical loads of various intensities, a universal tension/compression test stand is used. This machine allows the generation of uniaxial loadings up to 2500 N, which corresponds to stresses up to 50 MPa for a laminated sheet of cross section $S = 100 \times 0.5$ mm^2. A commercial tester was chosen to realize the mechanical excitation: the MECMESIN MultiTest-d 2.5 test bench that allows close control of the displacement due to a potentiometer having a resolution of 0.01 mm. The applied force is measured due to a commercial force gauge (MECMESIN BFG 2500N), with a resolution of 0.5 N ($\Leftrightarrow$0.01 MPa for the defined section S).

Now, as all aspects of the proposed magnetomechanical bench are exposed, design validation and results analysis can be performed, as presented in Section V.

V. Results

The magnetomechanical bench previously presented is based on a robust theory and design, allowing high repeatability rates and the application of a wide variety of waveforms. The measurement procedure plays an important role in obtaining a precise characterization of the material. In particular, demagnetization is a crucial step that needs to be periodically realized on the yoke and accomplished on the sample before and after each test. The procedure used in this work can be summarized in the following way—for a given excitation waveform, test frequency, and stress level, the material induction is elevated up to near-saturation and then slowly lowered (demagnetization stage); the material magnetization is once

TABLE III
COMMON TESTING CONDITIONS

Tested material	M530-50A grade Non-oriented material $e_{sh} = 0,5$ mm
Tested direction	Rolling Direction (RD)
Induced voltage waveform	Sinusoidal
$B_{p,i}$ [T]	[0,05:0,05:1,30]
Frequency f [Hz]	{1;5;10;20;50;100}
Stress σ [MPa]	{-20;-10;-5;0;+5;+10;+20}

more risen to saturation and then lowered using small steps according to the data to acquire; a second demagnetization is realized; and test conditions are changed, or the experiment ended. Such a procedure allows eliminating the presence of remanent induction that could cause an unwanted effect, thus enhancing the confidence in obtained results.

As a proof of concept, first, experiments are realized using a sinusoidal reference for a frequency range of [1; 100 Hz]. The low-frequency tests allow observing the quasistatic phenomenon of magnetomechanical coupling, while high-frequency tests offer an insight into the effects of mechanical loads on dynamical losses. All tests are realized following the so-called $\sigma - \vec{H}$ methodology, consisting of first applying a constant mechanical load to the sample and then subjecting it to a magnetizing field. The material used and the testing conditions are described in Table III.

Results obtained from the developed modified-SST on unstressed materials ($\sigma = 0$ MPa) are compared to some references obtained on a commercial Brockhaus MPG100 tester using both Epstein frame and standard SST, to prove the liability, precision, and representativeness of the measurements. The behavior under mechanical loads is then qualitatively analyzed and compared with the expected material response based on some considerations from the literature.

A. Validation for Unstressed Samples

Results obtained for unstressed samples are compared to some references originating from a commercial tester. Various frequencies are analyzed {5;10;50;100}Hz, showing good accordance between B–H curves of both apparatuses, as shown in Fig. 8.

Slight differences in the curves' shape can be observed. At low frequency, the loops obtained through the magnetomechanical bench tend to have a squared shape in comparison with the sigmoid shape of the loops originating from the Brockhaus tester. Nevertheless, this can be easily explained by the use of a direct magnetic field measurement (H-coil sensors) in comparison with indirect measures [28]. At high frequency and high induction, an important discrepancy can also be observed, and the origin of which is still unclear—additional analysis are being realized.

Furthermore, it can be observed that the curves obtained on the developed bench are quasiperfectly symmetrical in terms of induction and magnetic field and that inner curves are all included within the major B–H loop. This is not the case for results acquired on the commercial rig, denoting a better control of the measurement condition in the proposed experimental bench.

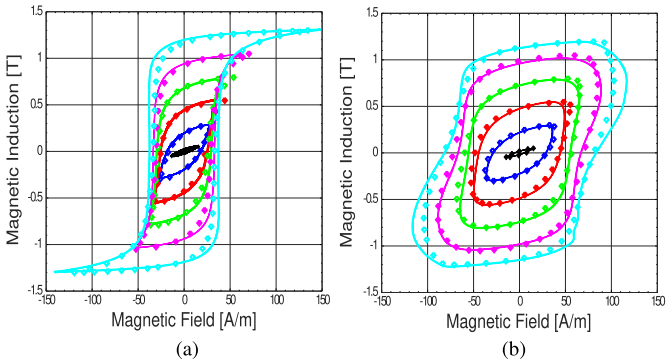

Fig. 8. Comparison of unstressed material behavior at (a) 5 and (b) 100 Hz obtained on the developed magnetomechanical bench (lines) and a Brockhaus tester (diamonds ◇).

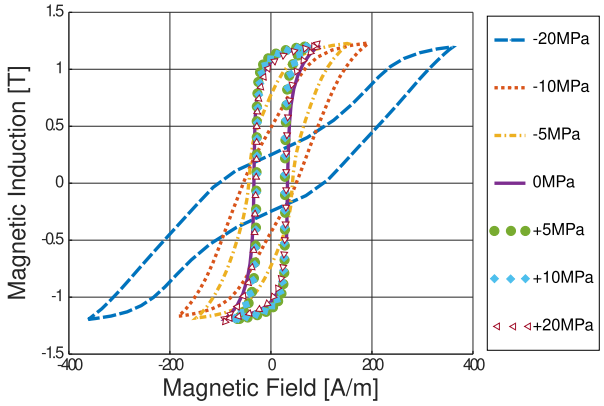

Fig. 9. Effect of tensile (+) and compressive (−) stresses on the quasistatic magnetic behavior at 1 Hz and 1.2 T.

B. Impact of Uniaxial Stress on Magnetic Properties

To assess the impact of stress on magnetic properties, one can primarily observe the global changes occurring on a B–H loop in the function of the applied load. Fig. 9 shows the effect of compressive and tensile stresses on the quasistatic magnetic hysteresis (1 Hz) for the tested material. Changes observed in hysteresis-curve forms due to the application of compressive and tensile stresses are coherent with anterior findings [34], [35].

If no strong changes are observed when tensile stresses are applied, this is not the case for compressive ones: indeed, in that case, even small levels of compression dramatically worsen the magnetic properties. A strong decrease of the B versus H slope is shown, denoting a fall in magnetic permeability, whereas the loop area increases, which means higher static losses. Those observations are consistent with previous analysis realized on the same type of material [36]. Focusing on the loops obtained under tensile loads, it is possible to observe that small levels of stress enhanced magnetic properties, slightly improving the permeability, and diminishing losses (decrease in the coercive field). However, as the stress

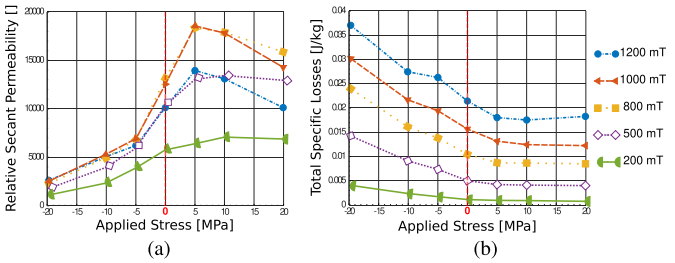

Fig. 10. Effect of stress on the relative secant permeability and specific total losses at 1 Hz. (a) μ_r. (b) W_{tot}.

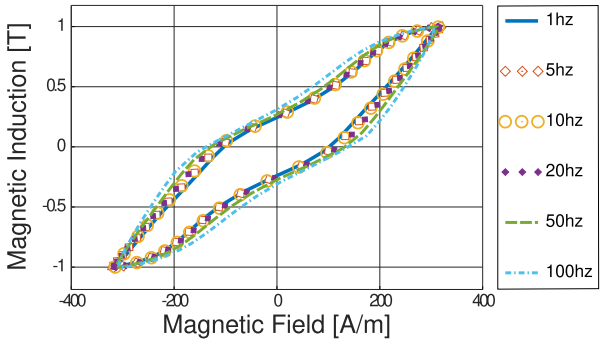

Fig. 11. Effect of a 20-MPa compressive stress on the magnetic losses of a sample tested at 1.0 T and frequencies from 1 to 100 Hz.

level increases, this behavior is reversed, and at +20 MPa, the effect of stress begins to worsen the magnetic properties. This nonmonotonic behavior of the material under tensile stress is in close accordance with earlier studies [35], [37]. That way, it can be said that the developed magnetomechanical bench is able to faithfully reproduce known experimental results, which are—at least qualitatively—in accordance with expected material behavior under stress.

The effect of stress on specific ferromagnetic properties of tested material can also be more closely analyzed. In Fig. 10(a), the evolution of the relative secant permeability μ_r in the function of applied external stress is presented for a sample tested at 1 Hz.

As highlighted previously, a strong decrease in permeability is observed when a compressive stress is imposed on the tested sample. However, tensile stress impact is nonmonotonous. Indeed, the material shows an increase in the permeability at low-stress levels, but as the tension intensity is raised, the behavior is reversed, and a decrease is observed. This negative impact of high-amplitude tensile stress on the permeability is stronger for high induction levels although already present on a smaller scale at 0.2 T for a stress amplitude of +20 MPa. Obtained experimental results are, thus, in accordance with previous observations realized on iron–silicon alloys [3]. In Fig. 10, the evolution of total losses at 1 Hz is shown. As seen previously, the material endures a strong increase in total losses when compression is applied and a small reduction of them for low tensile stress. For high-tension levels, no improvement is visible, and even a slight increase seems to appear for higher inductions, as already highlighted in [3], [4], and [38].

Measurements at higher frequencies show that the impact of mechanical loads on dynamic losses can be neglected in comparison with its effect on static ones (one to two orders of magnitude lower). However, an interesting point is that the relative contribution of dynamic losses in the total one's changes in function of the applied stress. At +20 MPa/100 Hz, dynamic losses account for more than 60% of total losses, whereas it represents less than 35% of those under high compression (−20 MPa/100 Hz). It is particularly visible in Fig. 11, where the frequency increase does not induce a significant variation of the loop area for a sample under strong compressive stress, whereas its impact on unstressed or positively stressed samples is way more noticeable [see Fig. 8(a) and (b)]. Those results are coherent with the ones obtained for a wide range of tensile stress levels in [38] and for compressive stresses in [4].

Such information can be extremely useful when optimizing the performance of electrotechnical machinery since it allows targeting specific material and/or structure arrangement and properties. One can for example add silicon content to a material in order to lower its conductivity if it is aimed to be used in an application involving tensile stress and high frequency. On the contrary, the structure and geometry of a rotating machine can be altered in order to lower the surge of high-intensity compressive stress in the direction of the magnetic field and, thus, diminish global losses observed at a fixed frequency.

VI. Conclusion

This article proposes a unidirectional magnetomechanical bench that follows international standards for magnetic measurements. It describes the different aspects of the bench, notably the closed-loop control used to ensure the induced voltage waveform and the advanced field measurement method employed to enhance precision and representativity. The mechanical aspects are also detailed, in particular the conception and geometry of a dedicated antibuckling fixture that allows imposing strong compressive stress levels onto thin sheet samples in a controlled fashion. Results for unstressed tests are compared to the ones obtained on a commercial bench under the same conditions, showing good accordance and, thus, validating the magnetomechanical bench design. Results under tensile and compressive stress are also shown, demonstrating close conformity with the literature and expected outcomes.

Experimental results obtained on the proposed magnetomechanical bench embrace a wide range of testing conditions, allowing their usage into numerical models. For example, they are currently used to test loss separation models, in order to evaluate their validity and the behavior of their parameters under magnetomechanical conditions. Studies are notably realized to propose some improvements to the well-known Steinmetz's law and ensure its consistency when stress is applied to magnetic material. Finally, the data obtained through this magnetomechanical SST are exploited in more complex models used in finite element modeling (FEM) [39].

They are necessary for parameter identification and the validation of models allowing the simulation of electromagnetic devices [40].

REFERENCES

[1] A. Moses, "Effects of applied stress on the magnetic properties of high permeability silicon-iron," *IEEE Trans. Magn.*, vol. MAG-15, no. 6, pp. 1575–1579, Nov. 1979.

[2] M. LoBue, C. Sasso, V. Basso, F. Fiorillo, and G. Bertotti, "Power losses and magnetization process in Fe–Si non-oriented steels under tensile and compressive stress," *J. Magn. Magn. Mater.*, vols. 215–216, pp. 124–126, Jun. 2000.

[3] D. Singh, P. Rasilo, F. Martin, A. Belahcen, and A. Arkkio, "Effect of mechanical stress on excess loss of electrical steel sheets," *IEEE Trans. Magn.*, vol. 51, no. 11, pp. 1–4, Nov. 2015.

[4] A. P. S. Baghel, J. B. Blumenfeld, L. Santandrea, G. Krebs, and L. Daniel, "Effect of mechanical stress on different core loss components along orthogonal directions in electrical steels," *Electr. Eng.*, vol. 101, no. 3, pp. 845–853, Sep. 2019.

[5] M. F. de Campos *et al.*, "Effect of rolling on the residual stresses and magnetic properties of a 0.5% Si electrical steel," *J. Magn. Magn. Mater.*, vol. 320, no. 14, pp. e377–e380, Jul. 2008.

[6] A. Schoppa, J. Schneider, and J.-O. Roth, "Influence of the cutting process on the magnetic properties of non-oriented electrical steels," *J. Magn. Magn. Mater.*, vols. 215–216, pp. 100–102, Jun. 2000.

[7] B. Y. Huang, K. Yamamoto, C. Kaido, and Y. Yamashiro, "Effect of cold-rolling on magnetic properties of non-oriented silicon steel sheets (Part II)," *J. Magn. Magn. Mater.*, vol. 209, nos. 1–3, pp. 197–200, Feb. 2000.

[8] L. Bernard and L. Daniel, "Effect of stress on magnetic hysteresis losses in a switched reluctance motor: Application to stator and rotor shrink fitting," *IEEE Trans. Magn.*, vol. 51, no. 9, pp. 1–13, Sep. 2015.

[9] Y. Kai, Y. Tsuchida, T. Todaka, and M. Enokizono, "Evaluation of local residual stress distribution of stator core in a rotating machine," *Electr. Eng. Jpn.*, vol. 181, no. 3, pp. 1–8, Nov. 2012.

[10] L. Bernard, X. Mininger, L. Daniel, G. Krebs, F. Bouillault, and M. Gabsi, "Effect of stress on switched reluctance motors: A magneto-elastic finite-element approach based on multiscale constitutive laws," *IEEE Trans. Magn.*, vol. 47, no. 9, pp. 2171–2178, Sep. 2011.

[11] K. Yamazaki, H. Mukaiyama, and L. Daniel, "Effects of multi-axial mechanical stress on loss characteristics of electrical steel sheets and interior permanent magnet machines," *IEEE Trans. Magn.*, vol. 54, no. 3, pp. 1–4, Mar. 2018.

[12] Z. Gmyrek, "Single sheet tester with variable dimensions," *IEEE Trans. Instrum. Meas.*, vol. 65, no. 7, pp. 1661–1668, Jul. 2016.

[13] L. Daniel and O. Hubert, "An analytical model for the Δ_E effect in magnetic materials," *Eur. Phys. J. Appl. Phys.*, vol. 45, no. 3, Mar. 2009, Art. no. 31101.

[14] O. Hubert and L. Daniel, "Measurement and analytical modeling of the ΔE effect in a bulk iron-cobalt alloy," *IEEE Trans. Magn.*, vol. 46, no. 2, pp. 401–404, Feb. 2010.

[15] *Standard Practice for Sampling and Procurement Testing of Magnetic Materials*, Standard A24/A34M-06, ASTM/International, 2012.

[16] M. Rekik, O. Hubert, and L. Daniel, "Influence of a multiaxial stress on the reversible and irreversible magnetic behaviour of a 3%Si–Fe alloy," *Int. J. Appl. Electromagn. Mech.*, vol. 44, nos. 3–4, pp. 301–315, Mar. 2014.

[17] V. Permiakov, "Measurement techniques for magnetic characterization of Fe–Si alloys," in *Proc. IEEE Instrum. Meas. Technol. Conf. (IMTC)*, Dec. 2006, pp. 742–746.

[18] Y. Kai, Y. Tsuchida, T. Todaka, and M. Enokizono, "Effect of local residual stress in rotating machine core on vector magnetic property," in *Proc. 19th Int. Conf. Electr. Mach. (ICEM)*, Sep. 2010, pp. 1–6.

[19] U. Aydin *et al.*, "Rotational single sheet tester for multiaxial magneto-mechanical effects in steel sheets," *IEEE Trans. Magn.*, vol. 55, no. 3, pp. 1–10, Mar. 2019.

[20] T. Kanada, Y. Kido, A. Kutsukake, T. Ikeda, and M. Enokizono, "Magnetic properties of soft magnetic materials under tensile and compressive stress," *Przegląd Elektrotechniczny*, vol. 87, no. 9b, pp. 93–96, 2011.

[21] *Standard Test Methods for Alternating-Current Magnetic Properties of Materials at Power Frequencies Using Sheet-Type Test Specimens*, Standard A804/A804M-04, ASTM/International, 2015.

[22] *Magnetic materials—Part 3: Methods of Measurement of the Magnetic Properties of Electrical Steel Strip and Sheet by Means of a Single Sheet Tester*, Standard IEC 60404-3, 2010.

[23] *Methods of Measurement of the Magnetic Properties of Electrical Steel Strip and Sheet by Means of a Single Sheet Tester*, Standard JIS C 2556, 2015.

[24] S. Tumanski, "A multi-coil sensor for tangential magnetic field investigations," *J. Magn. Magn. Mater.*, vols. 242–245, no. 2, pp. 1153–1156, Apr. 2002.

[25] N. J. Batistela, F. B. R. Mendes, N. Sadowski, P. Kuo-Peng, and J. P. A. Bastos, "A strategy for iron losses separation," in *Proc. Prog. Electromagn. Res. Symp.*, Pisa, Italy, 2004, pp. 413–416.

[26] N. J. Batistela and A. J. Perin, "A fixed frequency sliding mode control for voltage source inverter," in *Proc. 3rd Brazilian Power Electron. Conf. (COBEP)*, 1995, pp. 229–234.

[27] H. Pfützner and G. Shilyashki, "Theoretical basis for physically correct measurement and interpretation of magnetic energy losses," *IEEE Trans. Magn.*, vol. 54, no. 4, pp. 1–7, Apr. 2018.

[28] O. de la Barrière, C. Ragusa, M. Khan, C. Appino, F. Fiorillo, and F. Mazaleyrat, "A simple compensation method for the accurate measurement of magnetic losses with a single strip tester," *IEEE Trans. Magn.*, vol. 52, no. 5, pp. 1–4, May 2016.

[29] J. Nissen and L.-E. Paulsson, "Influence of field inhomogeneity in magnetic calibration coils," *IEEE Trans. Instrum. Meas.*, vol. 45, no. 1, pp. 304–306, Feb. 1996.

[30] B. J. Mailhe, R. de Araujo Elias, I. P. C. da Silva, N. Sadowski, N. J. Batistela, and P. Kuo-Peng, "Influence of shielding on the magnetic field measurement by direct H-coil method in a double-yoked SST," *IEEE Trans. Magn.*, vol. 54, no. 3, pp. 1–4, Mar. 2018.

[31] E. Carminati and A. Ferrero, "A virtual instrument for the measurement of the characteristics of magnetic materials," *IEEE Trans. Instrum. Meas.*, vol. 41, no. 6, pp. 1005–1009, Dec. 1992.

[32] J. W. Eaton, D. Bateman, S. Hauberg, and R. Wehbring. (2020). *GNU Octave Version 5.2.0 Manual: A High-Level Interactive Language for Numerical Computations*. Open Source. [Online]. Available: https://octave.org/doc/v5.2.0/

[33] E. de France. (2020). *Finite Element code_aster, Analysis of Structures and Thermomechanics for Studies and Research*. Open Source. [Online]. Available: https://www.code-aster.org/

[34] D. Miyagi, K. Miki, M. Nakano, and N. Takahashi, "Influence of compressive stress on magnetic properties of laminated electrical steel sheets," *IEEE Trans. Magn.*, vol. 46, no. 2, pp. 318–321, Feb. 2010.

[35] O. Perevertov, "Influence of the applied elastic tensile and compressive stress on the hysteresis curves of Fe-3%Si non-oriented steel," *J. Magn. Magn. Mater.*, vol. 428, pp. 223–228, Apr. 2017.

[36] C. S. Schneider, "Effect of stress on the shape of ferromagnetic hysteresis loops," *J. Appl. Phys.*, vol. 97, no. 10, p. 10E503, May 2005.

[37] O. Perevertov and R. Schäfer, "Influence of applied tensile stress on the hysteresis curve and magnetic domain structure of grain-oriented Fe–3%Si steel," *J. Phys. D, Appl. Phys.*, vol. 47, no. 18, May 2014, Art. no. 185001.

[38] N. Leuning, S. Steentjes, M. Schulte, W. Bleck, and K. Hameyer, "Effect of elastic and plastic tensile mechanical loading on the magnetic properties of NGO electrical steel," *J. Magn. Magn. Mater.*, vol. 417, pp. 42–48, Nov. 2016.

[39] L. Bernard, B. J. Mailhé, N. Sadowski, N. J. Batistela, and L. Daniel, "Multiscale approaches for magneto-elasticity in device simulation," *J. Magn. Magn. Mater.*, vol. 487, Oct. 2019, Art. no. 165241.

[40] L. Bernard, B. J. Mailhé, S. L. Ávila, L. Daniel, N. J. Batistela, and N. Sadowski, "Magnetic hysteresis under compressive stress: A multiscale-Jiles-Atherton approach," *IEEE Trans. Magn.*, vol. 56, no. 2, pp. 1–4, Feb. 2020.

Benjamin Joseph Mailhé received the M.Sc. degree in mechanical engineering with a specialization in material science from the Université de Technologie de Compiègne, Compiègne, France, in 2012, and the Ph.D. degree from the Electrical Engineering Department, Universidade Federal de Santa Catarina, Florianópolis, Brazil, in 2018.

He was part of the Grupo de Conceição e Análise de Dispositivos Electromagnéticos (GRUCAD), Universidade Federal de Santa Catarina. He is currently working as a Research Consultant for the ICREA Ingeniería Creativa, Bogotá, Colombia, acting as a link between the private sector and universities. His research interests include the experimental and numerical investigation of complex material behavior, as well as renewable technologies and their sociotechnical integration.

Laurent Didier Bernard received the M.Sc. degree from the Institut National Polytechnique de Grenoble, Grenoble, France, in 2004, and the Ph.D. degree from the École Centrale de Lyon, Écully, France, and the Universidade Federal de Minas Gerais (co-supervision), Belo Horizonte, Brazil, in 2007.

He worked several years as a Research Engineer with the Centre National de la Recherche Scientifique (CNRS), Laboratoire de Génie Électrique de Paris (LGEP), Gif-sur-Yvette, France. He is currently a Professor with the Grupo de Conceição e Análise de Dispositivos Electromagnéticos (GRUCAD), Universidade Federal de Santa Catarina, Florianópolis, Brazil. His research interests concern mesh-based numerical methods for electromagnetics and coupled problems.

Laurent Daniel (Member, IEEE) received the Ph.D. degree from the École Normale Supérieure de Cachan, Cachan, France, in 2003 and the Habilitation degree in physics from the Université Paris-Sud, Orsay, France, in 2011.

Since 2015, he has been a Full Professor with CentraleSupélec, Université Paris-Saclay, Gif-sur-Yvette, France. His research activities, within the Group of Electrical Engineering of Paris (GeePs), Paris, France, are dedicated to electromechanical and magnetomechanical couplings in materials for electrical engineering applications. He is notably involved in the definition of multiscale methods for the prediction of such coupled phenomena and in the development of dedicated experimental characterization setups. Since 2014, he has been the Director of the Automotive Mechatronics Chair, founded by Faurecia, Nanterre, France, the CentraleSupélec, and Esigelec, Saint-Étienne-du-Rouvray, France.

Nelson Sadowski (Senior Member, IEEE) received the B.Sc. and M.Sc. degrees in electrical engineering from the Universidade Federal de Santa Catarina (UFSC), Florianópolis, Brazil, in 1982 and 1985, respectively, and the Ph.D. and Habilitation degrees from the Institut National Polytechnique de Toulouse (INPT), Toulouse, France, in 1993 and 2000, respectively.

He is currently a Full Professor with the Grupo de Conceição e Análise de Dispositivos Electromagnéticos (GRUCAD), UFSC. He published two books and developed two software. His research interests embrace the calculation of electromagnetic fields and the development of finite element solutions for electrical machinery simulation.

Nelson Jhoe Batistela (Senior Member, IEEE) received the B.Sc. and M.Sc. degrees in electrical engineering and the Ph.D. degree from the Universidade Federal de Santa Catarina (UFSC), Florianópolis, Brazil, in 1992, 1994, and 2001, respectively.

He is currently a Full Professor with the Grupo de Conceição e Análise de Dispositivos Electromagnéticos (GRUCAD), UFSC. His research interests focus on magnetic loss estimation and modeling, as well as premature fault detection, efficiency estimation, and model parameters determination for electrical machines.